This article was downloaded by: [Brown University Library]
On: 01 January 2015, At: 22:10
Publisher: Taylor & Francis
Informa Ltd Registered in England and Wales Registered Number: 1072954 Registered office: Mortimer House, 37-41 Mortimer Street, London W1T 3JH, UK

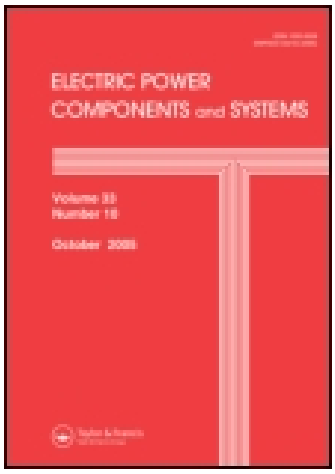

Electric Power Components and Systems
Publication details, including instructions for authors and subscription information:
http://www.tandfonline.com/loi/uemp20

Controller Design Using Ant Colony Algorithm for a Non-inverting Buck-Boost Chopper Based on a Detailed Average Model

Amir Masoud Bozorgi[a], Vahid Fereshtehpoor[b], Mohammad Monfared[a] & Navid Namjoo[a]
[a] PELab, Department of Electrical Engineering, Ferdowsi University of Mashhad, Mashhad, Iran
[b] Department of Electrical Engineering, Islamic Azad University, Science and Research Branch, Tehran, Iran
Published online: 31 Dec 2014.

CrossMark
Click for updates

To cite this article: Amir Masoud Bozorgi, Vahid Fereshtehpoor, Mohammad Monfared & Navid Namjoo (2015) Controller Design Using Ant Colony Algorithm for a Non-inverting Buck-Boost Chopper Based on a Detailed Average Model, Electric Power Components and Systems, 43:2, 177-188, DOI: 10.1080/15325008.2014.975385

To link to this article: http://dx.doi.org/10.1080/15325008.2014.975385

PLEASE SCROLL DOWN FOR ARTICLE

Taylor & Francis makes every effort to ensure the accuracy of all the information (the "Content") contained in the publications on our platform. However, Taylor & Francis, our agents, and our licensors make no representations or warranties whatsoever as to the accuracy, completeness, or suitability for any purpose of the Content. Any opinions and views expressed in this publication are the opinions and views of the authors, and are not the views of or endorsed by Taylor & Francis. The accuracy of the Content should not be relied upon and should be independently verified with primary sources of information. Taylor and Francis shall not be liable for any losses, actions, claims, proceedings, demands, costs, expenses, damages, and other liabilities whatsoever or howsoever caused arising directly or indirectly in connection with, in relation to or arising out of the use of the Content.

This article may be used for research, teaching, and private study purposes. Any substantial or systematic reproduction, redistribution, reselling, loan, sub-licensing, systematic supply, or distribution in any form to anyone is expressly forbidden. Terms & Conditions of access and use can be found at http://www.tandfonline.com/page/terms-and-conditions

Electric Power Components and Systems, 43(2):177–188, 2015
Copyright © Taylor & Francis Group, LLC
ISSN: 1532-5008 print / 1532-5016 online
DOI: 10.1080/15325008.2014.975385

Taylor & Francis
Taylor & Francis Group

Controller Design Using Ant Colony Algorithm for a Non-inverting Buck–Boost Chopper Based on a Detailed Average Model

Amir Masoud Bozorgi,[1] Vahid Fereshtehpoor,[2] Mohammad Monfared,[1] and Navid Namjoo[1]

[1]PELab, Department of Electrical Engineering, Ferdowsi University of Mashhad, Mashhad, Iran
[2]Department of Electrical Engineering, Islamic Azad University, Science and Research Branch, Tehran, Iran

Downloaded by [Brown University Library] at 22:10 01 January 2015

CONTENTS

1. Introduction
2. Linearized Average State-Space Model
3. Converter Transfer Function Analysis
4. Ant Colony Controller Design
5. Detailed Average Model of the Non-Inverting Buck–Boost Chopper
6. Conclusion
References

Abstract—In this article, the non-inverting buck–boost converter and its operation modes are scrutinized. The closed-loop stability of the converter in buck and boost modes is analyzed, and the necessity of using an appropriated controller is demonstrated. Then the application of an adapted ant colony optimization to design a feedback controller is proposed, and a controller based on its existing model is tuned. Simulation and experimental results obtained from the ant colony optimization designed controller are then compared with a controller designed with the classic method. Although the simulation and experimental results prove the efficiency of the proposed control approach, a significant difference between controller behavior in practice and simulation is obvious. Finding these differences, more detailed models, including all parasitic elements, in the buck and boost modes are derived. Applying the proposed model in controller design illustrates that the desired performance of the converter can be guaranteed with a simple proportional-integral (PI) controller. The suggested ant colony-based controller is again tuned based on the more detailed model, which improves the performance of the converter system even more. Furthermore, good agreement between analytical and experimental outputs validates the accuracy of the modeling and simulation.

1. INTRODUCTION

The widespread use of DC/DC power converters (DC choppers) in many applications, and the considerable attention to improve their performance, turn them into an important subject in power electronics. In many applications where DC/DC converters are employed, a wide operating range for input and output voltages should be provided. This requires both step-up and step-down operation modes, depending on the amplitude of input and output voltages [1–5]. The non-inverting buck–boost chopper [6, 7], shown in Figure 1, can meet these requirements as it can be used as a buck, buck–boost, or boost converter. Furthermore, the simple structure, low stress on switches, and positive polarity of output voltage distinguish it

Keywords: non-inverting buck–boost chopper, small-signal model, type III, proportional-integral, ant colony, state-space model, detailed average model
Received 8 August 2013; accepted 27 September 2014

Address correspondence to Mr. Vahid Fereshtehpoor, Department of Electrical Engineering, Islamic Azad University, Science and Research Branch, No. 1.79, Abomoslem Alley, Ahmadabad 1 St., Mashhad, Khorasan Razavi, Tehran, Iran. E-mail: v.fereshtehpoor@gmail.com

Color versions of one or more of the figures in the article can be found online at www.tandfonline.com/uemp.

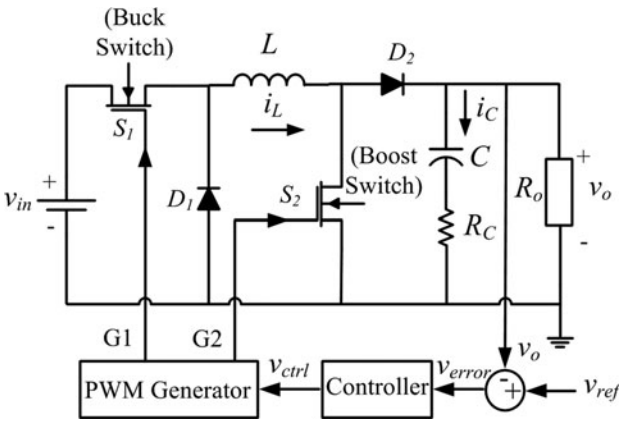

FIGURE 1. Non-inverting buck–boost chopper in presence of control system.

from other DC/DC structures, such as the Cuk converter [8], conventional buck–boost converter, and single-ended primary-inductance converter (SEPIC) [8, 9].

To study the performance of the converter in different operation modes, the first step is to obtain the model of the system for each mode of operation. A conventional solution to obtain a general and dynamic model of the system is the state-space average model. In [9–11], linearized state-space models for the buck, boost, and non-inverting buck–boost converters were introduced. In the boost operation mode, the chopper exhibits non-minimum phase characteristics, and the system will be unstable in the absence of an appropriate controller. Hence, the use of a proper closed-loop controller is of great importance. In recent years, various research was performed on applying the non-linear methods to control DC/DC converters [12–15]; however, the controller design approaches based on the linearized state-space average model, due to the simplicity of implementation and generality, maintain their popularity. While many classic controller design methods, either empirical or analytical techniques, have been presented to date, the intelligent design techniques have proven success in improving the performance of the controllers [16–20]. In [16], Sundareswaran and Sreedevi proposed a methodology to design a controller for the boost converter based on a colony of foraging honeybees. Afterward, they showed the application of modified particle swarm optimization (PSO) to the feedback controller design of the boost converter and compared it with the conventional one [17]. In [18, 19], the artificial immune system and foraging ants were applied to the boost converter. In this article, an adapted ant colony algorithm is employed to tune controller parameters for the non-inverting buck–boost chopper based on the currently available model of the converter [6]. Although the superior performance of the optimization method in comparison with the classic method is confirmed through simulations and experiments, there are obvious differences between simulation and experimental results.

To analyze the mismatch between the results, the reason behind the inaccuracy in the converter model should be investigated. In the case of power electronic converters, neglecting parasitic elements reduces the model accuracy. To ameliorate the accuracy of the linearized model, parasitic elements have been considered in the literature. In [21], the authors proposed a methodology to produce a rather accurate large-signal transient model for pulse-width modulation (PWM) DC/DC converters. The state-space average model of the buck–boost regulator in the presence of all system uncertainties was presented in [22].

In previous models presented for the non-inverting buck–boost chopper, only the effect of equivalent series resistance of the output capacitor has been considered. In this article, the more detailed model of the converter, considering all parasitic elements, is presented, and a general transfer function for the boost and buck modes is derived. Through the experimental tests, the accuracy of the presented model is proven. The proposed controller design methodology based on the more detailed model can successfully meet the specific design requirements in practice.

2. LINEARIZED AVERAGE STATE-SPACE MODEL

The non-inverting buck–boost chopper is a cascade combination of a buck and a boost converter, which has two switches, only one inductor, and a capacitor in its structure. DC/DC converters are often designed based on mathematical models. To achieve a certain performance objective, an accurate model is essential. To obtain the average state-space model of the non-inverting buck–boost converter, the switching strategy for two switches should be determined at first. In this converter, if both switches are driven with the same frequency and duty cycle, a quite similar performance to the conventional buck–boost converter will appear, and if the switches are driven with the same frequency but with different duty cycles, various operation modes can be attained. Consider the state when S_1 is switched and S_2 is continuously off during the switching period; in this case, the buck operation will be achieved. When S_1 is always on and S_2 is switched, the converter operates in the boost mode. The buck–boost operation mode should be avoided because of its high switching losses in comparison with the two other modes of operation. Table 1 summarizes the switching strategy in different operation modes.

Now, after determining the operation modes of the converter, the small-signal transfer functions, based on the state-space average method [6], can be derived as follows. For buck operation and only by including the equivalent series

Downloaded by [Brown University Library] at 22:10 01 January 2015

Downloaded by [Brown University Library] at 22:10 01 January 2015

Mode	S_1	S_2
Buck	Switching	Off
Boost	On	Switching
Buck–boost	Switching	Switching

TABLE 1. Switching strategy

resistance of capacitor (R_C), the small-signal transfer function of the control input ($\hat{d}$) and the source disturbance ($\hat{v}_{in}$) to the output voltage ($\hat{v}_o$) is

$$\hat{v}_o = \frac{\frac{V_{in}}{LC}(1 + R_C Cs)}{s^2 + \frac{s}{RC} + \frac{1}{LC}}\hat{d} + \frac{\frac{D_1}{LC}(1 + R_C Cs)}{s^2 + \frac{s}{RC} + \frac{1}{LC}}\hat{v}_{in}, \quad (1)$$

and for the boost operation, the small-signal transfer function is

$$\hat{v}_o = \frac{\frac{I_L}{C}\left(\frac{V_{in}}{LI_L} - s\right)(1 + R_C Cs)}{s^2 + \frac{s}{RC} + \frac{(1-D_2)^2}{LC}}\hat{d} + \frac{\frac{(1-D_2)}{LC}(1 + R_C Cs)}{s^2 + \frac{s}{RC} + \frac{(1-D_2)^2}{LC}}\hat{v}_{in}, \quad (2)$$

where R, C, and L are the load, capacitance, and inductance values of the circuit, respectively. D_1 and D_2 are duty cycles of S_1 and S_2 in the steady state, respectively. Furthermore, I_L is the inductor current, and V_{in} is the input voltage at the steady state. The quantities with a ˆ are small AC variations around the steady-state operating point.

3. CONVERTER TRANSFER FUNCTION ANALYSIS

3.1. Frequency Domain Analysis

One of the conventional methods to analyze the stability of a system is the frequency response analysis using the Bode diagram [23]. For the non-inverting buck–boost converter, according to the control method, if the ratio of the output voltage reference to the input voltage is lower than unity, the converter is in the buck mode, and when this ratio is higher than unity, the converter is in the boost mode of operation. Figure 2 depicts the Bode diagrams of the control (duty cycle) to the output for these two modes based on Eqs. (1) and (2) for the system parameters specified in Table 2.

V_{in}	9 V
V_o	7, 10, and 13 V
f_s	50 kHz
L	50 μH
R_o	2.5 and 1.67 Ω
C	1.8 mF

TABLE 2. Simulation and experimental parameters

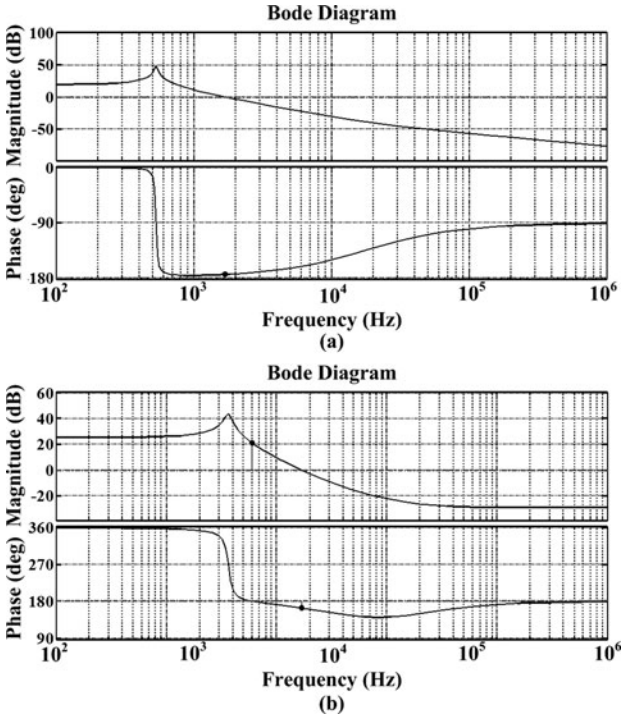

FIGURE 2. Bode diagrams of non-inverting buck–boost chopper: (a) buck mode (b) boost mode.

Figure 2 shows that the stability margins are favorable in the buck mode, but due to the negative phase and gain margins, the system is completely unstable in the boost mode. Hence, the controller is designed based on the boost transfer function. Carefully considering the transfer function, it can be found that a right-half-plane zero (RHPZ) is present, the location of which depends on the inductance value and also varies with inductance current and input voltage variations. The existence of an RHPZ in the transfer function of a system, according to the negative phase imposed to the system, leads to some limitation in choosing a wide bandwidth for the linear controller. The physical effect of this RHPZ was investigated in [11], as the fast rate of variation in duty cycle leads to undershoot in output voltage. This problem causes oscillation in output voltage.

The overall scheme of the converter circuit with the control system is shown in Figure 1. The measured output voltage is compared with the reference voltage, and the difference is fed into the controller. The PWM generator uses the controller output signal to determine the state of the switches.

Figure 3 depicts how switching pulses are generated from the controller output signal. The buck and boost switch states are determined by comparing two triangle carrier waveforms with the controller output. In this figure, V_{H1} and V_{L1} are maximum and minimum voltages of the carrier waveform in

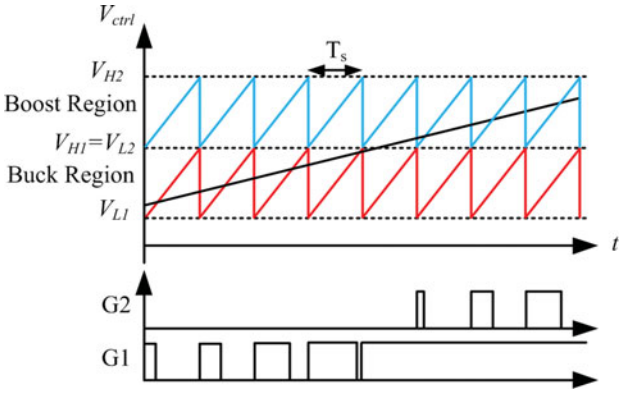

FIGURE 3. PWM generation strategy for buck and boost switches.

the buck region, and V_{H2} and V_{L2} are the same quantities in the boost region. $G1$ and $G2$ are generated pulses for S_1 and S_2, respectively.

3.2. Controller Selection and Design

The most serious problems with the open-loop converter system are (1) an inadequate phase margin that may lead to instability and (2) a zero type of system (due to the zero slip of magnitude diagram in low frequencies) resulting in a non-zero steady-state error. Thus, the controller should solve these problems. The proportional-integral (PI) and type III are two conventional linear controllers used for DC/DC converters [24]. Equations (3) and (4) show the transfer functions of PI and type III controllers, respectively.

$$C1(s) = K_p + \frac{K_i}{s}, \tag{3}$$

$$C2(s) = \frac{K_3 s^2 + K_2 s + K_1}{s(K_6 s^2 + K_5 s + K_4)}. \tag{4}$$

The pole at origin of these controllers provides a high gain at low frequencies and eliminates the steady-state error. In addition, the existence of zero in the transfer functions can improve the phase margin. According to the selected controller parameters, the performance of the closed-loop system will be determined. Various methods are available to determine the optimum controller parameters, and among them, the ant colony algorithm is one of the advanced and most recent techniques that have gained attention due to the benefits it offers.

4. ANT COLONY CONTROLLER DESIGN

4.1. Ant Colony Algorithm

The ant colony algorithm is an evolutionary meta-heuristic method used for a wide class of optimization problems, first introduced in [25]. The main idea of ant colony algorithm is to imitate real ants. The real ants find the shortest path from nest to food by using a material called pheromone. When an ant passes a path, it lays a trail of pheromones, which evaporates with time. The main idea is that in paths with longer length, the evaporation of pheromones is dominant; therefore, the pheromone density in shorter paths will increase gradually and more ants will be attracted to them until the shortest path is found from global cooperation among ants in the colony.

The ant colony algorithm models the problem as the search for a minimum cost path in a graph. Considering a list of cities, in each step, the kth ant moves from the rth city to a city among the candidate list of cities (sth city) based on a transition rule as

$$s = \begin{cases} \arg\max_{u \in u(k)} \left\{ [\tau_{ru}]^{\alpha} [\eta_{ru}]^{\beta} \right\} & \text{if } q \le q_0 \\ t & \text{otherwise} \end{cases}, \tag{5}$$

where

$u(k)$ is a list of next possible cities,
$.\tau_{ru}$ is the existing pheromone between the rth and uth city,
η_{ru} is the inverse distance between two cities,
q is a random variable uniformly distributed over [0,1],
q_0 is an arbitrary parameter in interval [0, 1], and
α and β are the weighting factors of τ_{ru} and η_{ru}, respectively.

If the constraint is true ($q \le q_0$), the city that maximizes the above argument is chosen; otherwise, the tth city that belongs to the candidate cities will be evaluated based on the probabilistic rule defined by Eq. (6), in which l is a member of $u(k)$:

$$P_{rt}^{k} = \frac{[\tau_{rt}]^{\alpha} [\eta_{rt}]^{\beta}}{\sum_{l \in u(k)} [\tau_{rl}]^{\alpha} [\eta_{rl}]^{\beta}}. \tag{6}$$

After calculation of the above probability function for each candidate city, the next city is selected by the Roulette wheel rule. As Eq. (6) shows, the transition rule is a tradeoff between pheromone density and visibility of ants (the length between two cities).

When all ants finish their tours, pheromone is updated on all edges as follows:

$$\tau_{rs} = \rho \tau_{rs} + \sum_{k=1}^{m} \Delta \tau_{rs}^{k}, \tag{7}$$

in which ρ is the evaporation coefficient of the pheromone trail ($\rho < 1$) and

$$\Delta \tau_{rs}^{k} = \begin{cases} \dfrac{Q}{L_k} & \text{if}(r,s) \in \text{tour done by ant } k \\ 0 & \text{otherwise} \end{cases}, \tag{8}$$

where Q is an arbitrary value, and L_k is the tour length passed by the kth ant.

Downloaded by [Brown University Library] at 22:10 01 January 2015

Downloaded by [Brown University Library] at 22:10 01 January 2015

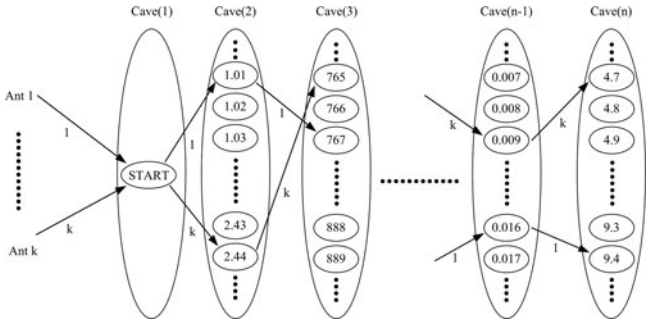

FIGURE 4. Graphical representation of ant colony algorithm for controller parameters tuning.

4.2. Application of Ant Colony to Tune the Controller Parameters

To adopt the ant colony algorithm to tune the controller parameters, the following steps should be followed.

Step 1: Create n caves and l_i cities inside the ith cave ($i = 2, \ldots, n$); $(n-1)$ is the number of parameters to be optimized by the algorithm, and l_i values must cover the range of variations of the ith parameter with the specified resolution (Figure 4).

Step 2: Generate m ants and put them in cave 1 (cave 1 is the start point and includes only one city).

Step 3: Each ant chooses only one city among the cities in the cave based on the rule in Eq. (6). Also, because distance is meaningless in designing a controller, η can be defined as

$$\eta_{rs} = Ae^{\frac{-\left|P_i(s)-P_{opt-i}\right|}{P_{opt-i}}}, \tag{9}$$

where $P_i(s)$ is the value of the sth city of the ith cave, and $P_{opt\text{-}i}$ is the optimum value of it, which is obtained from the best ant in recent iteration or from a classic method. Also, A is an arbitrary parameter.

Step 4: Repeat Step 3 for all parameters (caves).

Step 5: After the tour was completed, the pheromone is updated by Eqs. (7) and (8), with the difference that L_k is the value of the objective function.

Step 6: If the convergence criteria are not met, return to Step 1; otherwise, the algorithm is finished.

To obtain a desired performance in the time domain, the following constraint should be met:

$$f = t_r + t_s + O.S + U.S \tag{10}$$

subject to

$$t_r < 0.01(\text{sec}), \tag{11}$$

$$t_s < 0.05(\text{sec}), \tag{12}$$

$$O.S < 5\%, \tag{13}$$

$$U.S < 5\%, \tag{14}$$

k_1, k_2, k_3, and k_4	4, 4, 1000, and 1000
P_1, P_2	2, 1
Number of cave cities	200
Iterations	200
Number of ants	50
α, β, ρ, Q, and q_0	1, 2, 0.9, 10, and 0.5

TABLE 3. Initial information of ant colony algorithm

in which t_r and t_s are rise time and settling time of the step response of the closed-loop system, respectively; also OS and US denote the overshoot and undershoot of the step response, respectively. Considering the type of compensated system, which is for both PI and type III controllers, the steady-state error is zero, and as a result, it is eliminated from the objective function.

Using the techniques commonly referred to as transformation methods, one can eliminate the constraints by augmenting them into the original objective function [26, 27]. Removing the above constraints, the objective function becomes

$$f = k_1\left(\frac{O\,S}{0.05}\right)^{P_2} + k_2\left(\frac{U\,S}{0.05}\right)^{P_2} + k_3\left(\frac{t_s}{0.05})\right)^{P_1} + k_4\left(\frac{t_r}{0.01})\right)^{P_1}. \tag{15}$$

In the above equation k_1 to k_4 and exponents P_1 and P_2 are weighting factors obtained through preliminary sample runs of the optimization algorithm and are listed in Table 3. Also, the number of ants and other algorithm parameters (α, β, ρ, Q, q_0) are typical values in ant colony algorithms [25].

To compare the performance of ant colony optimization (ACO) with other heuristic algorithms, and to show the proper rate of convergence, PSO and genetic algorithm (GA) are chosen. The objective function is as Eq. (15), and the initial parameters of the algorithms are summarized in Tables 4 and 5. As Figure 5 reveals, the adapted ACO can reach better results in the same iterations in comparison with the two other methods. Based on this, other simulation and experimental tests are performed only with ACO.

4.3. Discussion of Simulation and Experimental Results

The PI and type III controllers are tuned by the ant colony algorithm subject to minimizing Eq. (15) for the transfer func-

Number of population	50
Iterations	200
P_c, P_m, and e	0.9, 0.05, and 5

TABLE 4. Initial information of GA

Downloaded by [Brown University Library] at 22:10 01 January 2015

Swarm size	50
Iterations	200
w_{min}	0.4
w_{max}	0.9
C_1	2.05
C_2	2.05
r_1	$U \sim [0, 1]$
r_2	$U \sim [0, 1]$

TABLE 5. Initial information of PSO algorithm

tion of the converter in the boost mode. The input data of the algorithm are listed in Table 3. The range of each controller parameter is determined based on the location of poles and zeros of the system and the stability criteria. To evaluate the superiority of the ant colony-based controllers, their performance is compared to the controllers designed based on the frequency response technique [23]. The parameters of PI and type III controllers obtained from the ant colony and classic methods, as well as their time- and frequency-domain characteristics calculated from the small-signal model, are summarized in Tables 6 and 7, respectively.

The circuit of Figure 1 is simulated in MATLAB/Simulink (The MathWorks, Natick, Massachusetts, USA). To better represent the real-world system, practical issues, such as digital sampling effect and converter switching, are included in the simulations. A sampling frequency of 50 kHz has been adopted, and the TUSTIN method has been used to discretize the controller. The simulated waveforms in response to a 3-V rising and 6-V falling step in the reference voltage are depicted in Figure 6. Compared to the classic method, the ant colony algorithm offers a significant improvement in tuning both PI and type III controller parameters. While the controllers tuned by the ant colony provide better performance than the classic tuned ones, the ant colony-based type III compensated system exhibits the superior performance in comparison with the PI in terms of faster response and less oscillations.

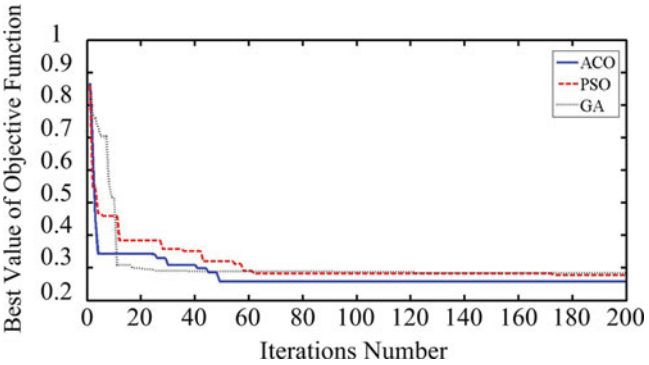

FIGURE 5. Comparison of convergence trend for three different evolutionary algorithms: ACO, PSO, and GA.

To investigate the performance of the controllers in practice, they are applied to the experimental setup, as shown in Figure 7, including a 1-kW non-inverting buck–boost chopper, an eZdspTMS320F28335 (Spectrum Digital, USA) as the processor, and the loads. The experimental parameters are the same as simulation parameters given in Table 2. Figure 8 illustrates experimental waveforms when the reference voltage changes from 10 to 13 V and then to 7 V for PI and type III controllers, respectively. In this figure, t_{tr} shows the transient time. Having examined the results, one can see that controllers' dynamic performance is different in the practice and simulation. It seems that the lack of accuracy in the converter model can be a reason for this unexpected behavior. In the following section, the more detailed state-space model of the converter will be derived.

5. DETAILED AVERAGE MODEL OF THE NON-INVERTING BUCK–BOOST CHOPPER

5.1. Detailed Transfer Function of the Converter

To obtain a more detailed model of the converter, the converter circuit in Figure 9, is considered, in which R_c denotes the capacitor resistance, R_L is the resistance of the inductance, and R_D and R_S show conducting mode resistance of diodes and switches, respectively.

For the boost mode, by considering $[i_L, v_C]$ as the state variables and by writing the Kirchhoff's voltage law (KVL) equations for the loops of Figure 9(a), the state-space model for the conduction time can be written as

$$\begin{cases} \dot{x} = A_1 x + B_1 u \\ y = C_1 x + D_1 u \end{cases}, \tag{16}$$

$$x = \begin{bmatrix} i_L \\ v_C \end{bmatrix}, u = v_{in}, y = v_o, \tag{17}$$

$$A_1 = \begin{bmatrix} \frac{-1}{L}(2R_S + R_L) & 0 \\ 0 & \frac{-1}{\Delta} \end{bmatrix}, \tag{18}$$

$$B_1 = \begin{bmatrix} \frac{1}{L} & 0 \\ 0 & \frac{-R_o}{\Delta} \end{bmatrix}, \tag{19}$$

$$C_1 = \begin{bmatrix} 0 & 1 - \frac{CR_C}{\Delta} \end{bmatrix}, \tag{20}$$

$$D_1 = \begin{bmatrix} 0 & \frac{-CR_C R_o}{\Delta} \end{bmatrix}, \tag{21}$$

in which $\Delta = R_o C + R_C C$.

Output parameter	Simplified		More detailed	
	Classic	Ant colony	Classic	Ant colony
K_p	0.000886	0.000432	0.006617	0.027864
K_i	5.01	9.95	37.42	60.69
t_r (sec)	0.02400	0.00924	0.00225	0.00132
t_s (sec)	0.0420	0.0308	0.0039	0.0021
OS (%)	0	1.62	0	0
US (%)	0	0	0.1	0.3
PM (degrees)	90.5	89.6	69.8	69.4
GM (dB)	9.65	3.57	18.7	21.6
BW (Hz)	14.9	29.8	92.6	157

TABLE 6. PI controller tuned by ant colony and classic methods

Output parameter	Simplified		More detailed	
	Classic	Ant colony	Classic	Ant colony
K_1	20.29	101.45	78.50	107.68
K_2	0.05052	0.04761	0.11180	0.07927
K_3	3.146*e*–5	4.346*e*–5	3.977*e*–5	1.769*e*–5
K_4	1	1.47	1	1.43
K_5	8.3*e*–5	0.0001856	0.0002847	0.0003032
K_6	1.723*e*–9	6.63*e*–13	2.026*e*–8	6.8*e*–12
t_r (sec)	0.000328	0.000426	0.0005	0.0012
t_s (sec)	0.0159	0.00271	0.0045	0.0018
OS (%)	0	0	0.295	0
US (%)	2.35	1.66	1.1	0.7
PM (degrees)	46	129	63	69.6
GM (dB)	14.4	19.6	9.88	23.7
BW (Hz)	698	188	402	193

TABLE 7. Type III controller tuned by ant colony and classic methods

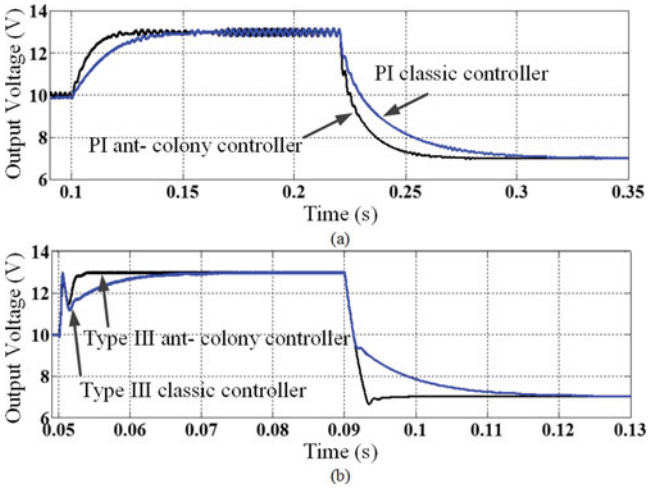

FIGURE 6. Output voltage simulation for simplified model in the presence of: (a) PI controllers and (b) type III controllers.

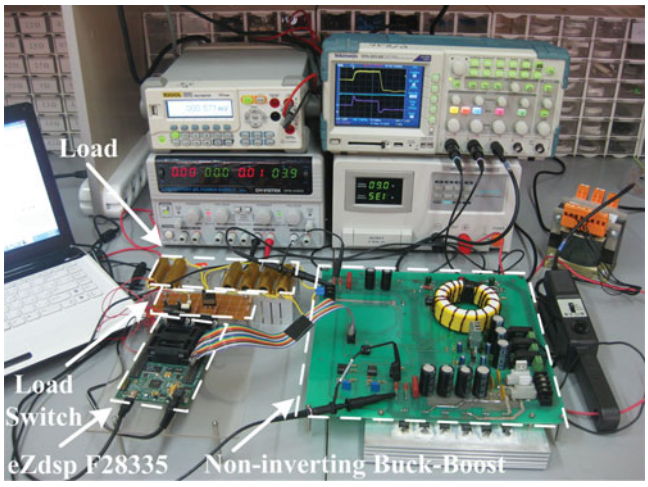

FIGURE 7. Experimental setup for non-inverting buck–boost chopper.

Downloaded by [Brown University Library] at 22:10 01 January 2015

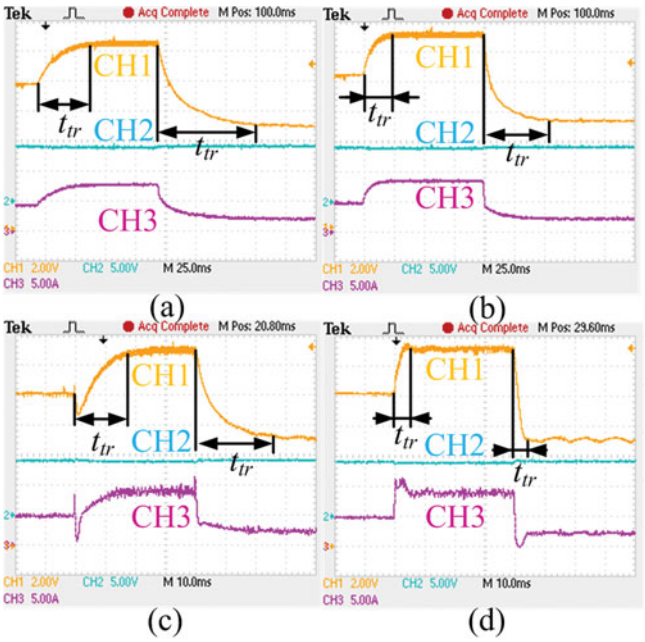

FIGURE 8. Experimental waveforms (CH1: output voltage, CH2: input voltage, CH3: input current) for designed controllers based on simplified model: (a) PI classic controller, (b) PI ant colony controller, (c) type III classic controller, and (d) type III ant colony controller.

To simplify the equations, the following assumptions are considered

$$\begin{aligned} R_{S1} &= R_{S2} = R_S, \\ R_{D1} &= R_{D2} = R_D. \end{aligned} \tag{22}$$

For the blocking period (Figure 9(b)), the equations will be as follows:

$$\begin{cases} \dot{x} = A_2 x + B_2 u \\ y = C_2 x + D_2 u \end{cases}, \tag{23}$$

$$A_2 = \begin{bmatrix} \dfrac{-1}{L}\left(R_S + R_L + R_D + \dfrac{CR_CR_o}{\Delta}\right) & \dfrac{1}{L}\left(\dfrac{CR_C}{\Delta} - 1\right) \\ \dfrac{R_o}{\Delta} & \dfrac{-1}{\Delta} \end{bmatrix}, \tag{24}$$

$$B_2 = \begin{bmatrix} \dfrac{1}{L} & \dfrac{CR_CR_o}{L\Delta} \\ 0 & \dfrac{-R_o}{\Delta} \end{bmatrix}, \tag{25}$$

$$C_2 = \begin{bmatrix} R_o - \dfrac{CR_o^2}{\Delta} & \dfrac{CR_o}{\Delta} \end{bmatrix}, \tag{26}$$

$$D_2 = \begin{bmatrix} 0 & \dfrac{CR_o^2}{\Delta} - R_o \end{bmatrix}. \tag{27}$$

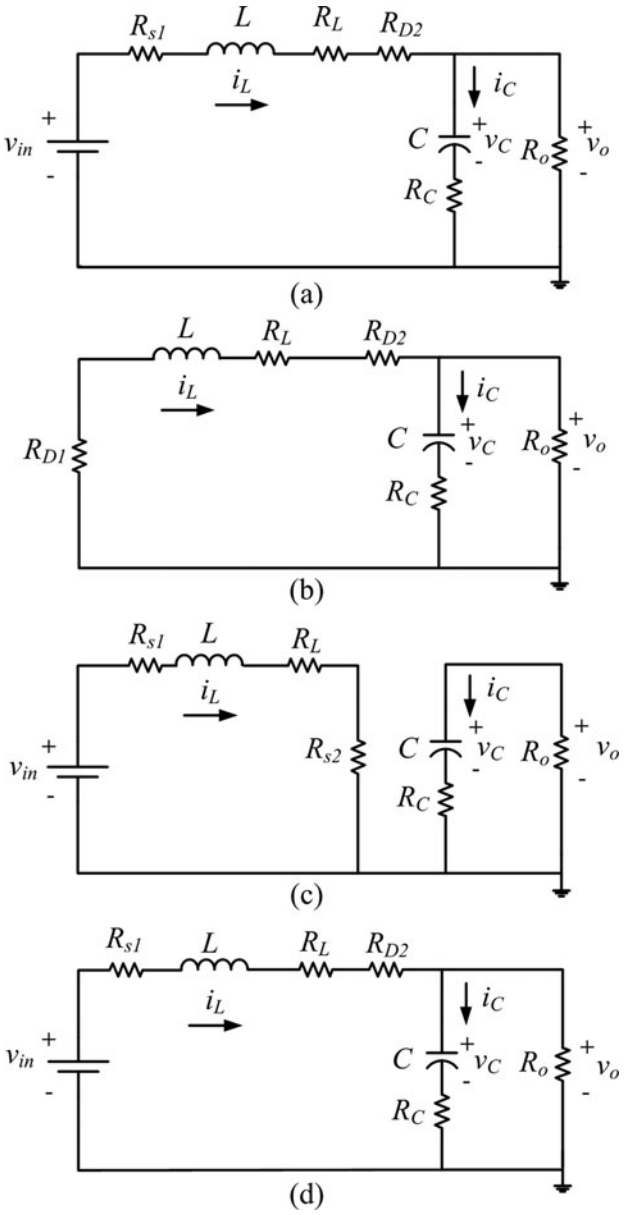

FIGURE 9. Equivalent circuit of the converter with parasitic elements for: (a) buck mode when buck switch conducts, (b) buck mode when buck switch blocks, (c) boost mode when boost switch conducts, and (d) boost mode when boost switch blocks.

To obtain the average model, the conduction and blocking-time equations are combined as follows:

$$\begin{cases} \dot{x}_P = A_P x + B_P u \\ y_P = C_P x + D_P u \end{cases}, \tag{28}$$

$$\begin{cases} A_P = A_1 d + A_2(1-d) \\ B_P = B_1 d + B_2(1-d) \\ C_P = C_1 d + C_2(1-d) \\ D_P = D_1 d + D_2(1-d) \end{cases}. \tag{29}$$

Downloaded by [Brown University Library] at 22:10 01 January 2015

Downloaded by [Brown University Library] at 22:10 01 January 2015

To specify x around the operating point, the following equation can be used:

$$\dot{x} = A_P x + B_P u = 0 \Rightarrow X = -A_P^{-1} B_P U. \quad (30)$$

Finally, to linearize the system, the static part (a fixed DC level) and small variations around the operating point should be decoupled as

$$\begin{cases} x(t) &= X + \hat{x} \\ d(t) &= D + \hat{d} \\ u(t) &= U + \hat{u} \\ v_o(t) &= V_o + \hat{v}_o \end{cases}. \quad (31)$$

Substituting Eq. (31) into Eq. (28) yields

$$\begin{cases} \dot{X} + \dot{\hat{x}} = A_P \hat{x} + B_P \hat{u} + [A_{12} X + B_{12} U]\hat{d} + \dot{X} \\ \dot{V}_o + \dot{\hat{v}}_o = C_P \hat{x} + D_P \hat{u} + [C_{12} X + D_{12} U]\hat{d} + \dot{V}_o \end{cases}, \quad (32)$$

where

$$\begin{cases} A_{12} = A_1 - A_2 \\ B_{12} = B_1 - B_2 \\ C_{12} = C_1 - C_2 \\ D_{12} = D_1 - D_2 \end{cases}. \quad (33)$$

Therefore, the output voltage variations can be expressed as

$$\hat{v}_o = [C_P(SI - A_P)^{-1}(A_{12}X + B_{12}U) + (C_{12}X + D_{12}U)]\hat{d} + (C_P(SI - A_P)^{-1}B_P + D_P)\hat{u}. \quad (34)$$

Assuming that $\hat{d}$ is the only control parameter, and after some tedious manipulations, the complete transfer function of the converter in the boost mode can be derived as

$$\begin{aligned} G(s) &= \frac{\hat{v}_o}{\hat{d}} = \frac{a_3 s^2 + a_2 s + a_1}{b_3 s^2 + b_2 s + b_1} \\ a_3 &= -V_{in} C L R_C D' \\ a_2 &= -V_{in} L \\ a_1 &= V_{in}(R_o D'^2 - R_L) \\ b_3 &= CL(R_o D'^2 + R_D + R_L) \\ b_2 &= CR_C R_o(-3DD' + 1) \\ &\quad + CR_o D'(R_D D'^2 + R_S + R_L D') + LD'^2 \\ b_1 &= 2R_D(-3DD' + 1) - 4R_L D + 2R_L + R_o D'^4, \end{aligned} \quad (35)$$

where $D\prime = 1 - D$ and

$$D = \frac{(V_o - V_{in} + R_S + R_D + R_L)I_L}{(R_S I_L - V_o - R_D I_L)}, \quad (36)$$

in which I_L can be substituted from Eq. (30);

$$I_L = \frac{V_{in}\Delta}{d^2(R_o\Delta - CR_C R_o) + d(\Delta(-R_D - 2R_o + R_s) + CR_C R_o) + \Delta(R_D + R_L + R_o + R_s)}. \quad (37)$$

To simplify the final transfer function, lower-order terms were neglected with a good approximation.

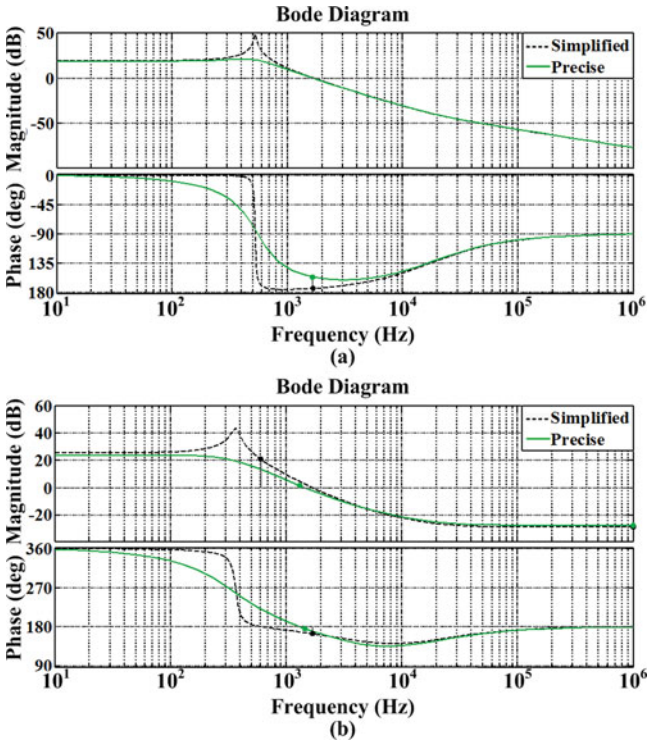

FIGURE 10. Bode diagrams of simplified and detailed model: (a) buck mode and (b) boost mode.

Carrying out the same operation for the buck mode, the transfer function would be

$$G(s) = \frac{\hat{v}_o}{\hat{d}} = \frac{a_2 s + a_1}{b_3 s^2 + b_2 s + b_1}$$

$$\begin{aligned} a_2 &= CR_C V_{in}(2R_D + R_L + R_o), \\ a_1 &= V_{in}(2R_D + R_L + R_o), \\ b_3 &= CL(R_C + R_o + R_L + R_D(2 - D) + R_S D), \\ b_2 &= C(R_D(R_D D' + (2D - D^2)R_o) + R_L(R_L + R_o + 4R_D) \\ &\quad + R_o(R_S D + (D' - D)R_C)) + L, \\ b_1 &= 2(2 - D)R_D + 2R_L + R_o. \end{aligned} \quad (38)$$

and

$$D = \frac{V_o + (2R_D + R_L)I_L}{V_{in} + (R_D - R_S)I_L}. \quad (39)$$

To compare the difference between the above-derived and simplified models, the Bode diagrams of the converter transfer function for the considered parameters are compared in Figure 10. It is obvious that the damping and stability margins of the system in the presence of parasitic elements have improved.

R_L	100 mΩ
R_C	5 mΩ
$R_{S1} = R_{S2}$	7.8 mΩ
$R_{D1} = R_{D2}$	80 mΩ

TABLE 8. Parasitic parameters

5.2. Discussion of Simulation and Experimental Results for Detailed Model

To analyze the performance of the more detailed model of the system, classic and ant colony controllers are again designed based on this model. The main elements of the system are as shown in Table 2, and other parasitic values are summarized in Table 8. In the test rig, two parallel diodes were used instead of a single diode, and each diode on time resistance is 0.08 Ω; hence, their equivalent value has been imposed in the calculations. In addition, R_L has been calculated by considering the resistance of printed circuit board (PCB) tracks and the resistor increase originating from the skin effect in the switching frequency of 50 kHz. Figure 11 shows the behavior of output voltage in presence of PI and type III designed controllers in response to the output voltage reference variations. As Figure 11 depicts, after a 3-V jump in the boost mode, the converter goes to buck mode with a 6-V fall in the output voltage reference. To verify the consistency of simulated controllers' behavior, the same tests were conducted on the experimental setup. As Figures 12 and 13 show, with a good approximation, the controllers' real performance agrees with the simulation results. Furthermore, the performance of the system in the presence of controllers based on a detailed model has dramatically improved. In other words, the ability of designing a better controller based on the more detailed model of the system shows the usefulness of the model. The superior behavior of the controllers tuned by the ant colony algorithm confirms the proposed controller design methodology. To demonstrate the robustness of the ant colony designed controllers, a step change in the output power has been applied. In this test, two 10-Ω resistors are paralleled to the load with a switch. The small transition change on the output voltage validates the robustness of the designed controllers.

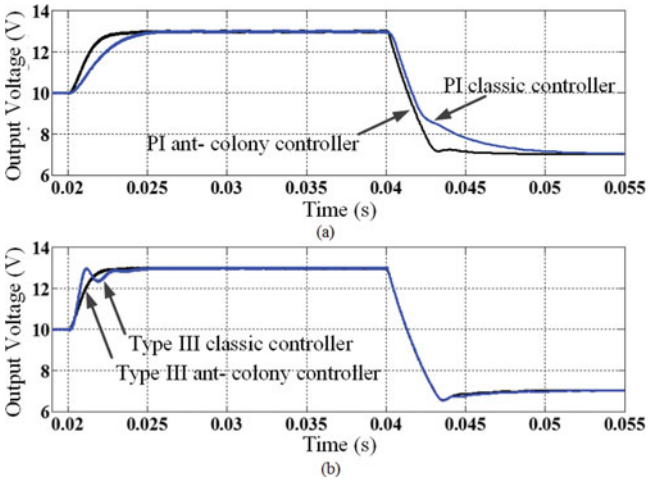

FIGURE 11. Output voltage simulation for more detailed model in presence of: (a) PI controllers and (b) type III controllers.

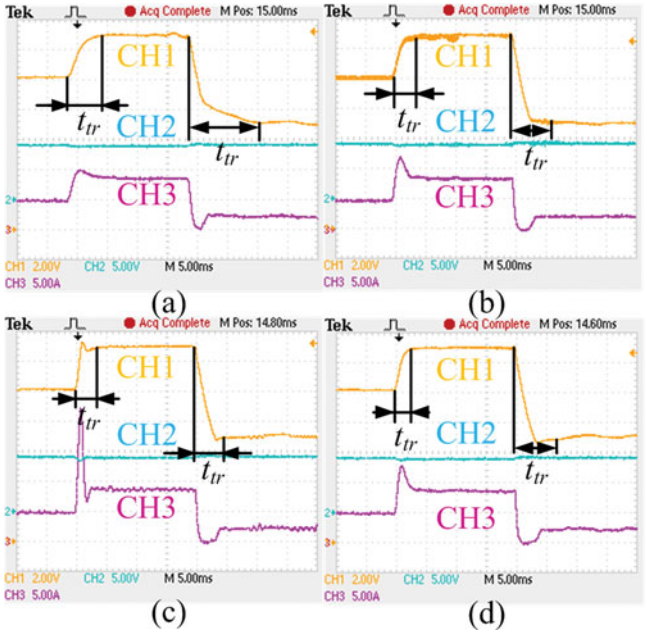

FIGURE 12. Experimental waveforms (CH1: output voltage, CH2: input voltage, CH3: input current) for designed controllers based on more detailed model: (a) PI classic controller, (b) PI ant colony controller, (c) type III classic controller, and (d) type III ant colony controller.

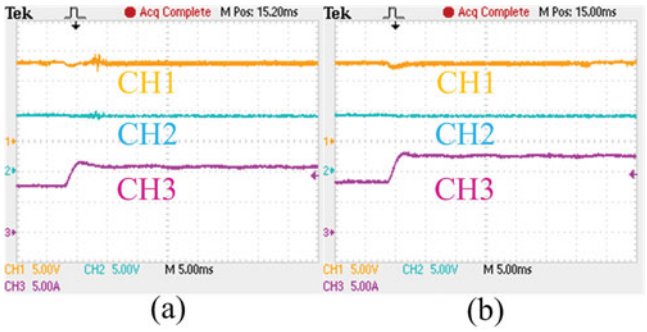

FIGURE 13. Experimental waveforms in response to step load change (CH1: output voltage, CH2: input voltage, CH3: input current) for designed controllers based on more detailed model: (a) PI ant colony controller and (b) type III ant colony controller.

Downloaded by [Brown University Library] at 22:10 01 January 2015

Downloaded by [Brown University Library] at 22:10 01 January 2015

6. CONCLUSION

In this article, the non-inverting buck–boost chopper and its operation modes were investigated, and the necessity of designing a proper controller to guarantee the stability of the converter system in boost mode has been demonstrated. Then, the application of the ant colony algorithm to tune the controller parameters of the converter was proposed. PI and type III controllers were tuned by classic and ACO methods. Despite a considerable improvement in the response of the ant colony-based controller compared to the classic one, the difference of experimental and simulation results demonstrated the necessity of obtaining a more detailed model of the converter. Therefore, a more detailed model of the converter considering the effect of all parasitic elements in buck and boost modes is obtained. As the results show, designing the controllers based on the more detailed transfer function of the system can dramatically improve the performance of the closed-loop system. The more detailed transfer function of the converter can be useful for future research about this converter.

REFERENCES

[1] Sahu, B., and Rincon-Mora, G. A., "A low voltage, dynamic, noninverting, synchronous buck–boost converter for portable applications," *IEEE Trans. Power Electron.*, Vol. 19, pp. 443–452, 2004.

[2] Xiao, H., and Xie, S., "Interleaving double-switch buck-boost converter," *IET Power Electron.*, Vol. 5, pp. 899–908, 2012.

[3] Schaltz, E., Rasmussen, P. O., and Khaligh, A., "Non-inverting buck-boost converter for fuel cell applications," *Proceedings of 34th Annual IEEE Industrial Electronics IECON Conference*, Orlando, FL, 10–13 November 2008.

[4] STMicroelectronics, "An MCU-based low cost non-inverting buck-boost converter for battery chargers," Application Report AN2389, 2007.

[5] Sayed, K., Abdel-Salam, M., Ahmed, A., and Ahmed, M., "New high voltage gain dual-boost DC-DC converter for photovoltaic power systems," *Elect. Power Compon. Syst.*, Vol. 40, pp. 711–728, 2012.

[6] Lee, Y. J., Khaligh, A., and Emadi, A., "A compensation technique for smooth transitions in a noninverting buck–boost converter," *IEEE Trans. Power Electron.*, Vol. 24, pp. 1002–1015, 2009.

[7] Jingquan, C., Maksimovic, D., and Erickson, R. W., "Analysis and design of a low-stress buck-boost converter in universal-input PFC applications," *IEEE Trans. Power Electron.*, Vol. 21, pp. 320–329, 2006.

[8] Lefeuvre, E., Audigier, D., Richard, C., and Guyomar, D., "Buck-boost converter for sensorless power optimization of piezoelectric energy harvester," *IEEE Trans. Power Electron.*, Vol. 22, pp. 2018–2025, 2007.

[9] Mohan, N., Undeland, T. M., and Robbins, W. P., *Power Electronics Converters, Applications, and Design*, 3rd ed., Hoboken, NJ: Wiley, pp. 161–199, 2003.

[10] Middlebrook, R. D., and Cuk, R. S., "A general unified approach to modeling switching converter power stages," *IEEE PESC Record*, Cleveland, OH, 8–10 June 1976.

[11] Erickson, R., and Maksimovic, D., *Fundamental of Power Electronics*, 2nd ed., New York: Springer, pp. 185–289, 2000.

[12] Guoa, L., Hungb, J. Y., and Nelmsb, R. M., "Comparative evaluation of sliding mode fuzzy controller and PID controller for a boost converter," *Elect. Power Syst. Res.*, Vol. 81, pp. 99–106, 2011.

[13] Guoa, L., Hungb, J. Y., and Nelmsb, R. M., "Design of a fuzzy controller using variable structure approach for application to DC–DC converters," *Elect. Power Syst. Res.*, Vol. 83, pp. 104–109, 2012.

[14] Safari, S., Ardehali, M. M., and Sirizi, M. J., "Particle swarm optimization based fuzzy logic controller for autonomous green power energy system with hydrogen storage," *Energy Convers. Manag.*, Vol. 65, pp. 41–49, 2013.

[15] Oucheriah, S., "PWM-based adaptive sliding mode control for the boost converter with unknown parameters" *Int. J. Electron. Lett.*, Vol. 2, pp. 92–99, 2014.

[16] Sundareswaran, K., and Sreedevi, V. T., "Design and development of feed-back controller for a boost converter using a colony of foraging bees," *Elect. Power Compon. Syst.*, Vol. 37, No. 5, pp. 465–477, 2009.

[17] Sundereswaran, K., and Devi, V., "Application of a modified particle swarm optimization technique for output voltage regulation of boost converter," *Elect. Power Compon. Syst.*, Vol. 39, No. 3, pp. 288–300, January 2011.

[18] Sundereswaran, K., Devi, V., and Shrivastava, N. A., "Design and development of a feedback controller for boost converter using artificial immune system," *Elect. Power Compon. Syst.*, Vol. 39, No. 10, pp. 1007–1018, 2011.

[19] Sundareswaran, K., and Devi, V., "Feedback controller design for a boost converter through a colony of foraging ants," *Elect. Power Compon. Syst.*, Vol. 40, pp. 672–690, 2012.

[20] Krohling, R. A., and Rey, J. P., "Design of optimal disturbance rejection PID controllers using genetic algorithms," *Trans. Evolution. Computat.*, Vol. 5, pp. 78–82, 2001.

[21] Davoudi, A., and Jatskevich, J., "Realization of parasitics in state-space average-value modeling of PWM DC–DC converters," *IEEE Trans. Power Electron.*, Vol. 21, pp. 1142–1147, 2006.

[22] Modabbernia, M., Kohani, F., Fouladi, R., and Nejati, S., "The state-space average model of buck- boost switching regulator including all of the system uncertainties," *Int. J. Comput. Sci. Eng. (IJCSE)*, Vol. 5, pp. 120–132, 2013.

[23] Ogata, K., *Modern Control Engineering*, 5th ed., New Jersey: Prentice Hall, 2010.

[24] Shiau, J. K., and Cheng, C. J., "Design of a non-inverting synchronous buck-boost DC/DC power converter with moderate power level," *Robot. Comput.-Integrat. Manufact.*, Vol. 26, pp. 263–267, 2010.

[25] Dorigo, M., Maniezzo, V., and Colorni, A., "Ant system, optimization by a colony of cooperating agents," *IEEE Trans. Syst.*, Vol. 26, pp. 29–41, 1996.

[26] Ravindran, A., Ragsdell, K. M., and Reklaitis, G. V., *Engineering Optimization: Methods and Applications.* Hoboken, NJ: Wiley, pp. 260–330, 2006.

[27] Mehrizi-Sani, A., and Filizadeh, S., "An optimized space vector modulation sequence for improved harmonic performance," *IEEE Trans. Indust. Electron.*, Vol. 56, pp. 2894–2903, 2009.

BIOGRAPHIES

Amir Masoud Bozorgi received his B.S. and M.Sc. in electrical engineering from Ferdowsi University of Mashhad, Mashhad, Iran, in 2010 and 2013, respectively. His current research interests include modeling and control of power electronics converters, photovoltaic energy systems, and artificial intelligence applied to power electronics.

Vahid Fereshtehpoor received his M.Sc. in electrical engineering from the Science & Research Branch of Islamic Azad University, Tehran, Iran, in 2012. His current research interests include modeling and control of power electronics converters and renewable energy systems.

Mohammad Monfared received his B.Sc. in electrical engineering from Ferdowsi University of Mashhad, Iran, in 2004 and his M.Sc. and Ph.D. (both with honors) in electrical engineering from Amirkabir University of Technology, Tehran, Iran, in 2006 and 2010, respectively. He is currently an assistant professor at Ferdowsi University of Mashhad, Iran. His research interests include power electronics, motor drives, renewable energy systems, energy conversion, and control and applications.

Navid Namjoo was born in 1988 and received his B.Sc. in electrical engineering from Ferdowsi University of Mashhad, Mashhad, Iran. He obtained his M.Sc. in electrical engineering from Shahrood University of Technology in 2013. At present, he is working at Sun and Air Research Institute as a professional electrical system designer in the field of wind turbines. His research interests include power electronics, renewable energy, and control of on-grid converters.

Downloaded by [Brown University Library] at 22:10 01 January 2015